Article:
Subramanian, Pallavi, Gargani, Sofia, Palladini, Alessandra et al. (27 more authors) (2021) The RNA binding protein HuR is a gatekeeper of liver homeostasis. Hepatology. ISSN 0270-9139

https://doi.org/10.1002/hep.32153

Article type : Original Article

The RNA binding protein HuR is a gatekeeper of liver homeostasis

Pallavi Subramanian[1,15,#], Sofia Gargani[2,#], Alessandra Palladini[3,4], Margarita Chatzimike[2], Michal Grzybek[3,4], Mirko Peitzsch[1], Anastasios D. Papanastasiou[5,6], Iryna Pyrina[1], Vasileios Ntafis[2], Bettina Gercken[1], Mathias Lesche[7], Andreas Petzold[7], Anupam Sinha[1], Marina Nati[1], Veera Raghavan Thangapandi[8], Ioannis Kourtzelis[1,9,10], Margarita Andreadou[2], Anke Witt[1], Andreas Dahl[7], Ralph Burkhardt[11], Robert Haase[12], António Miguel de Jesus Domingues[12], Ian Henry[12], Nicola Zamboni[13], Peter Mirtschink[1], Kyoung-Jin Chung[1], Jochen Hampe[8], Ünal Coskun[3,4], Dimitris L. Kontoyiannis[2,14,15,*], Triantafyllos Chavakis[1,3,4,9,15,*]

[1]Institute for Clinical Chemistry and Laboratory Medicine, Faculty of Medicine, Technische Universität Dresden, Dresden, Germany; [2]Biomedical Sciences Research Centre 'Alexander Fleming', Division of Immunology, Vari, Greece; [3]Paul Langerhans Institute Dresden, Helmholtz Zentrum München, University Hospital and Faculty of Medicine, Technische Universität Dresden, Dresden, Germany; [4]German Center for Diabetes Research (DZD e.V.), Neuherberg, Germany; [5]Department of Biomedical Sciences, University of West Attica, Athens, Greece; [6]Biomedical Sciences Research Center 'Alexander Fleming', Histopathology Unit, Vari, Greece; [7]DRESDEN-concept Genome Center, Center for Molecular and Cellular Bioengineering, Technische Universität Dresden, Dresden, Germany; [8]Department of Internal Medicine I, University Hospital and Faculty of Medicine, Technische Universität Dresden, Dresden, Germany; [9]National Center for Tumor Diseases, Partner Site Dresden, Dresden and German Cancer Research Center, Heidelberg, Germany; [10]Hull York Medical School, York Biomedical Research Institute, University of York, York, UK; [11]Institute of Clinical Chemistry and Laboratory Medicine, University Hospital Regensburg, Regensburg, Germany; [12]Scientific Computing Facility, Max Planck Institute of Molecular Cell Biology and Genetics, Dresden, Germany; [13]Institute of Molecular Systems Biology, ETH Zurich, Zurich, Switzerland; [14]Aristotle University of Thessaloniki, School of Biology, Department of Genetics, Development & Molecular Biology, Thessaloniki, Greece.

This article has been accepted for publication and undergone full peer review but has not been through the copyediting, typesetting, pagination and proofreading process, which may lead to differences between this version and the Version of Record. Please cite this article as doi: 10.1002/HEP.32153

[#] equal contribution as first authors, * equal contribution as senior authors

Word count: 5993 (Introduction/Methods/Results/Discussion/Author contributions/Acknowledgments/References).

Excluded from word count: Title page, abstract, key words, abbreviations, financial support and figures legends.

KEYWORDS

HuR, Elavl1, NAFLD, NASH, hepatocellular carcinoma, liver, steatosis, RNA-binding protein, triglycerides, lipid metabolism, bile acid, FXR

[15]Corresponding authors:

Triantafyllos Chavakis

Institute for Clinical Chemistry and Laboratory Medicine

University Clinic Carl Gustav Carus, Technische Universität (TU) Dresden

Fetscherstraße 74, 01307 Dresden

Phone: +49 351 458 2109, Email: triantafyllos.chavakis@uniklinikum-dresden.de

Pallavi Subramanian

Institute for Clinical Chemistry and Laboratory Medicine

University Clinic Carl Gustav Carus, Technische Universität (TU) Dresden

Fetscherstraße 74, 03017 Dresden

Phone: +49 351 4586250, Email: pallavi.subramanian@uniklinikum-dresden.de

Dimitris L. Kontoyiannis

Biomedical Sciences Research Centre 'Alexander Fleming', Division of Immunology

Vari 16672, Greece

Phone: Tel: +30 210 9654335, Email: kontoyiannis@fleming.gr

FINANCIAL SUPPORT

This work was supported in part by grants from the European Research Council (DEMETINL to TC), the Else Kröner Fresenius Stiftung (2014_A30 to PS), the Medical

Faculty, Technische Universität Dresden (MeDDriveGrant-60409 to PS) and by the InfrafrontierGR/Phenotypos (MIS 5002135) project.

ABBREVIATIONS

NAFLD, nonalcoholic fatty liver disease; NASH, non-alcoholic steatohepatitis; HCC, hepatocellular carcinoma; TAG, triglycerides; RBP, RNA binding proteins; *Elavl1*, embryonic lethal abnormal vision like 1; HSC, hepatic stellate cell; ND, normal diet; IPA, Ingenuity Pathway Analysis; GSEA, Gene Set Enrichment Analysis; CM, conditioned medium; BA, bile acid; FXR, farnesoid X-activated receptor; CTNNB1, β-catenin; AST, aspartate aminotransferase; ALT, alanine aminotransferase; CE, cholesterol ester; RNA-seq, RNA sequencing; RNP, ribonucleoprotein; RIP-seq, RNP-immunoprecipitation and RNA sequencing; WT, wildtype; TCDCA, taurochenodeoxycholic acid; TUDCA, tauroursodeoxycholic acid; TMCA α+β, tauromuricholic acid (alpha+beta); TCA, taurocholic acid; ER, endoplasmic reticulum; UPR, unfolded protein response; AFP, alpha-fetoprotein; OPN, osteopontin; Jag1, jagged1.

DATA AVAILABILITY

RNA sequencing data and RIP-sequencing data are available at GEO with the accession IDs GSE143358 and GSE143703.

ABSTRACT

BACKGROUND AND AIMS: Non-alcoholic fatty liver disease (NAFLD) is initiated by steatosis and can progress via fibrosis and cirrhosis to hepatocellular carcinoma (HCC). The RNA binding protein HuR controls RNAs at the posttranscriptional level; hepatocyte HuR has been implicated in the regulation of diet-induced hepatic steatosis. The present study aimed to understand the role of hepatocyte-HuR in NAFLD development and progression to fibrosis and HCC.

APPROACH AND RESULTS: Hepatocyte-specific HuR-deficient mice and control HuR-sufficient mice were fed either a normal diet or a NAFLD-inducing diet. Hepatic lipid accumulation, inflammation, fibrosis and HCC development were studied by histology, flow cytometry, quantitative PCR and RNA sequencing. The liver lipidome was characterized by lipidomics analysis and the HuR-RNA interactions in the liver were mapped by RNA immunoprecipitation-sequencing. Hepatocyte-specific HuR-deficient mice displayed spontaneous hepatic steatosis and fibrosis predisposition, compared to control HuR-sufficient mice. On a NAFLD-inducing diet, hepatocyte-specific HuR-deficiency resulted in exacerbated inflammation, fibrosis and HCC-like tumor development. A multi-omic approach, including lipidomics, transcriptomics and RNA-immunoprecipitation sequencing revealed that HuR orchestrates a protective network of hepatic-metabolic and lipid homeostasis-maintaining pathways. Consistently, HuR-deficient livers accumulated, already at steady-state, a triglyceride signature resembling that of NAFLD livers. Moreover, upregulation of *Spp1* and its product osteopontin mediated, at least partially, the fibrosis development in hepatocyte-specific HuR deficiency on a NAFLD-inducing diet, as shown by experiments utilizing antibody blockade of osteopontin.

CONCLUSIONS: HuR is a gatekeeper of liver homeostasis preventing NAFLD-related fibrosis and HCC, suggesting that the HuR-dependent network could be exploited therapeutically.

INTRODUCTION

Nonalcoholic fatty liver disease (NAFLD) affecting up to 30% of the adult population and 70-80% of obese and diabetic individuals, is associated with dysfunctional hepatic metabolism (1, 2). NAFLD ranges from simple intrahepatic fat accumulation (steatosis), to non-alcoholic steatohepatitis (NASH), which is characterized by hepatocyte death and inflammation and may progress to fibrosis, cirrhosis and hepatocellular carcinoma (HCC) (1, 3). Hepatic fibrosis is the main factor determining liver-related mortality in NASH patients (4).

Excessive triglyceride (TAG) accumulation is the initiating process of NAFLD (5). Both, plasma non-esterified fatty acids and fatty acids from *de novo* lipogenesis are utilized for TAG synthesis in the liver (5). Liver TAG can be stored as lipid droplets in hepatocytes, secreted as very-low-density-lipoprotein particles or hydrolyzed (6). A network of enzymes and transcription factors controls hepatic metabolic pathways (2). RNA binding proteins (RBP) are integral to the post-transcriptional regulation of gene expression in the liver under physiological and pathological conditions (7, 8). However, less is known about the cell type-specific function of RBPs in the liver, particularly in hepatocytes.

The RBP HuR (encoded by *Elavl1*; embryonic lethal abnormal vision like 1), regulates gene expression post-transcriptionally by altering the abundance and use of RNAs that it binds to. HuR is present in the nucleus and in the cytoplasm; however, the most predominant functions of HuR are associated with its cytoplasmic localization (9, 10). Cytoplasmic HuR can promote the stability and translation of mRNAs containing uridine or adenine/uridine rich elements in their untranslated termini, although in some cases HuR may act in an opposite manner (10, 11). ShRNA-mediated HuR silencing in the liver attenuates hepatic stellate cell (HSC) activation and fibrosis development following bile duct ligation (12), and HuR is involved in TGF-β1-induced HSC activation (13). Hepatocyte HuR regulates hepatic steatosis development in response to high fat diet feeding (14). However, an in-depth analysis of the role of hepatocyte HuR in regulating NAFLD progression to fibrosis and HCC development is missing.

We identified HuR here as a master regulator of hepatic homeostasis. Hepatocyte-specific HuR deletion led to spontaneous steatosis and fibrosis predisposition. Upon feeding a NAFLD-inducing diet, hepatocyte-specific HuR-deficient mice developed heightened inflammation and fibrosis, which resulted in HCC-like tumor development. Mechanistic analysis revealed that HuR regulates a protective hepatic network of mRNAs, thereby sustaining hepatic metabolic and lipid homeostasis.

METHODS

Mouse experiments

Mice with hepatocyte-specific deletion of HuR (HuR^{HepKO}) in the C57BL/6 background were derived by crossing mice with a floxed *Elavl1* allele with mice expressing Cre recombinase under the control of Albumin promoter (Albumin-Cre). Cre-negative littermate mice with *Elavl1* floxed alleles (HuR^{WT}) were used as controls.

HuR^{WT} or HuR^{HepKO} mice were fed a methionine-low, choline-deficient high fat diet (60% kcal from fat, 0.1% methionine and choline-deficient diet; 60%-HFD-CD; A06071302, Research Diets) for 2 or 6 weeks or a normal diet (ND, 10% kcal fat, normal methionine and choline, A08051501, Research Diets) for 6 weeks. Long-term feedings were performed with a choline-deficient high fat diet (45% kcal from fat; CD-HFD-45%; D05010402, Research Diets) for up to 14 months. 7-10 week old mice of both genders were used. Animal experiments were approved by the prefecture of Attica, Greece and by the Landesdirektion Sachsen, Germany; animals received humane care according to the 'Guide for the care and use of laboratory animals'.

Statistical analysis

For analysis, the GraphPad Prism software (GraphPad Inc., La Jolla, CA) was used, unless otherwise stated in the Methods. For comparison of two groups, Mann-Whitney U test was used. Statistics for tumor incidence was calculated using two-tailed Fisher's exact test. Statistical analysis for lipidomics and RNA sequencing is described in the respective sections (in Supplemental Material). Data are expressed as mean±s.e.m. Significance was set at $P < 0.05$.

Detailed methods are in the Supplemental Material.

RESULTS

Hepatocyte-specific HuR deletion in mice promotes hepatic steatosis and fibrosis

To assess the function of HuR in hepatocytes, we generated mice with hepatocyte-specific HuR deletion (HuR^{HepKO}). Littermate Cre-negative *Elavl1* floxed mice (HuR^{WT}) were used as controls. Efficient HuR deletion was found in livers of HuR^{HepKO} mice (Figure-S1). Mice were fed a normal diet (ND) for 6 weeks (designated 'steady-state') or

NAFLD-inducing diets. Hepatocyte-specific HuR deficiency resulted in spontaneous hepatic steatosis at steady-state (Figure-1A). To clarify if the enhanced steatosis in HuR^{HepKO} mice at steady-state was metabolically benign (15) or predisposed to NASH and fibrosis, we fed HuR^{WT} and HuR^{HepKO} mice a NAFLD-inducing diet (methionine-low, choline-deficient high fat diet, with 60% kcal from fat (60%-HFD-CD)) for 2 or 6 weeks, representing early and advanced NAFLD/NASH development, respectively. Both HuR^{WT} and HuR^{HepKO} mice on 60%-HFD-CD developed steatosis (Figure-1B). However, hepatocyte-specific HuR deficiency exacerbated NAFLD-related fibrosis, as assessed by picrosirius red staining of livers upon 2 and 6 weeks of 60%-HFD-CD feeding (Figure-1C-D). Moreover, hydroxyproline concentration was increased in livers of HuR^{HepKO} mice, compared to control mice, upon 6 weeks of 60%-HFD-CD feeding (Figure-1E). We found enhanced mRNA expression of fibrosis-related factors, such as genes encoding different collagen subtypes as well as *Sphk1, Pdgfd, Pdgfb, Pdgfrb, Timp2, Igf1r, Tgfb2* and *Tgfb1*, in HuR^{HepKO} livers compared to HuR^{WT} livers (Figure-1F).

Analysis of fibrosis development owing to hepatocyte-specific HuR deletion

To provide mechanistic insights for the fibrosis development resulting from hepatocyte HuR deletion, we performed RNA sequencing (RNA-seq) of livers from HuR^{HepKO} and HuR^{WT} mice at steady-state. Hepatocyte HuR deficiency resulted in downregulation of 456 genes and upregulation of 593 genes (Figure-2A). Ingenuity Pathway Analysis (IPA) revealed that the hepatic fibrosis/HSC activation pathway was the most prominently enriched one in the significantly upregulated genes of HuR^{HepKO} livers (Figure-2B). Significantly enhanced expression of several genes involved in the hepatic fibrosis/HSC activation pathway was found in HuR^{HepKO} livers, compared to HuR^{WT} livers (Figure-2C and Figure-S2A). Several pathways related to hepatic fibrosis, such as the PDGF signaling pathway, epithelial mesenchymal transition pathway and hepatic fibrosis signaling pathway, were enriched in the significantly upregulated genes of HuR^{HepKO} livers relative to HuR^{WT} livers (Figure-2B). Gene Set Enrichment Analysis (GSEA) over the Molecular Signatures Database displayed a positive correlation between hepatocyte-specific HuR deficiency and extracellular matrix-associated gene expression and epithelial-mesenchymal transition-associated gene expression in the liver (Figure-2D-E and Supplemental table-1). Moreover, we assessed the crosstalk between hepatocytes

and HSCs *in vitro*. Conditioned medium (CM) derived from HuR-deficient hepatocytes promoted the expression of profibrotic genes, such as *Acta2*, *Col1a1*, *Col3a1*, *Col6a3* and *Timp2*, in wildtype HSCs, compared to treatment with CM from HuR^{WT} hepatocytes (Figure-S2B). Together, hepatocyte-specific HuR deficiency promotes HSC activation, thereby contributing to fibrosis predisposition of HuR^{HepKO} livers.

IPA revealed overrepresentation of several pathways in the significantly downregulated genes of HuR^{HepKO} livers, including cholesterol biosynthesis pathways (Figure-2F). The protective bile acid (BA)-activated FXR/RXR pathway was also enriched in the significantly downregulated genes of HuR-deficient livers (Figure-2F-G). The FXR (farnesoid X-activated) receptor pathway regulates lipid homeostasis and protects against liver fibrosis (1, 16-19). FXR activation in hepatocytes increases triglyceride clearance and blocks SREBP1-mediated lipogenesis, whereas FXR signaling in HSCs inhibits their activation and protects against fibrogenesis (1, 17, 20). IPA also revealed enrichment of the retinol biosynthesis pathway in the significantly downregulated genes of HuR-deficient livers (not shown); hence potentially decreased retinoic acid levels may further contribute to reduced FXR/RXR activation in HuR-deficient hepatocytes (21).

Analysis by qRT-PCR for selected genes, identified as differentially expressed due to hepatocyte-specific HuR deficiency by RNA-seq, confirmed upregulation of expression of genes involved in the hepatic fibrosis/hepatic stellate cell activation pathway and downregulation of expression of genes involved in the FXR/RXR activation pathway (Figure-2H).

Collectively, hepatocyte HuR deficiency promotes transcriptomic alterations culminating to HSC activation and fibrosis (Figure-2C-E), thereby underlying the fibrosis predisposition of HuR^{HepKO} mice at steady-state and leading to exacerbated fibrosis upon feeding a NAFLD-inducing diet.

Hepatocyte-specific HuR deletion promotes HCC-like tumor development

NAFLD-related fibrosis predisposes to HCC (3). We found that the tumor microenvironment pathway was enriched in the significantly upregulated genes in

HuR^{HepKO} livers compared to HuR^{WT} livers at steady-state (Figure-2B). Furthermore, the RNA-seq data obtained from HuR^{WT} and HuR^{HepKO} livers of steady-state mice were subjected to upstream regulator analysis using the IPA software (Supplemental table-2 and Figure-S3). The β-catenin (CTNNB1) pathway, involved in HCC pathogenesis (22), was predicted to be activated in HuR^{HepKO} livers, compared to HuR^{WT} livers (Supplemental table-2 and Figure-S3). Although HuR expression is increased in HCC and various other cancers and correlates with parameters of tumor progression (23), our data show that at steady-state and in NAFLD, HuR contributes to maintenance of hepatocyte homeostasis.

To study whether the predisposition towards hepatic steatosis and fibrosis due to hepatocyte-specific HuR-deficiency may promote NASH-related cancer development, we fed HuR^{HepKO} and HuR^{WT} mice with another NAFLD-inducing choline-deficient, high fat diet (with 45% kcal from fat, designated CD-HFD-45% hereafter) for up to 14 months. We chose the milder CD-HFD-45% model (24), as it displays a slower progression of liver disease pathogenesis, resembling the chronicity that governs the development of sequelae of human NAFLD, such as HCC. Plasma levels of aspartate aminotransferase (AST) and alanine aminotransferase (ALT) were elevated in HuR^{HepKO} mice compared to HuR^{WT} mice, following the CD-HFD-45% feeding (Figure-3A-B), indicating enhanced liver injury. HuR^{HepKO} livers showed an increased NASH activity score and exacerbated fibrosis, compared to HuR^{WT} livers (Figure-3C-D). Strikingly, a portion of HuR^{HepKO} (9/54) but no HuR^{WT} (0/27) mice developed HCC-like tumors, as assessed histo-pathologically (Figure-3E-F). The positive AFP (alpha-fetoprotein) staining (Figure-3G), together with the characteristic absence of reticulin staining (Figure-3H) in the tumor tissues of HuR^{HepKO} mice further underlined the resemblance to HCC (25, 26). Hepatic inflammation was increased in HuR-deficient mice compared to control mice, as assessed histologically (Figure-4A). Flow cytometry analysis for immune cell populations in the liver revealed significant increases in the numbers of $CD8^+$ T cells ($CD8^+CD4^-$ cells), $NK1.1^+$ NKT cells ($CD4^-CD8^-NK1.1^+$) and infiltrating macrophages ($Gr1^-CD11b^+CD11c^-$ $MHCII^+Ly6c^+$) (Figure-4B-G and Figure-S4). Together, HuR^{HepKO} mice on long-term feeding with the CD-HFD-45% exhibit more inflammation and fibrosis ultimately leading

to HCC-like tumor development, hence recapitulating the complete sequence of NAFLD-related pathogenesis and sequelae.

A NAFLD-like hepatic lipid signature owing to hepatocyte HuR deficiency

To further discern the spontaneous steatosis predisposing to fibrosis due to hepatocyte-specific HuR deficiency, we performed shotgun lipidomic analysis of livers obtained from HuR^{HepKO} and HuR^{WT} mice fed a ND or a 60%-HFD-CD. Shotgun lipidomics allow for detailed analysis of storage (triacylglycerides, TAG; cholesterol ester, CE) and non-storage lipids (all lipid classes other than TAG and CE). Consistent with the histological analysis (Figure-1A), the percentage of storage lipids was higher in HuR^{HepKO} livers compared to HuR^{WT} livers fed a ND (Figure-5A). Analysis of the lipid classes demonstrated that CEs and TAGs were enhanced in HuR^{HepKO} livers compared to HuR^{WT} livers (Figure-5B). Both, non-storage lipids and storage lipids of the two groups on ND separated from each other in the principal component analysis (Figure-5C-D). Since the storage lipids were enhanced in the absence of hepatocyte HuR, we further studied alterations in storage lipids species. The abundance of several TAG and CE species was upregulated in the absence of HuR (Figure-5E). When comparing the lipidome of livers of HuR^{WT} mice, which were fed either a 60%-HFD-CD or a ND, we found that 60%-HFD-CD feeding also led to increased TAG and CE levels (Figure-S5A-C). Furthermore, several TAG and CE species were enriched in NAFLD livers, compared to healthy livers of HuR^{WT} mice (Figure-5F).

All TAG species and some CE species, which were significantly increased at steady-state in HuR^{HepKO} livers (Figure-5E, bars outlined in red) were also upregulated in HuR^{WT} livers upon 60%-HFD-CD feeding (Figure-5F, bars outlined in red). Specifically, TAG_48:0, TAG_50:1, TAG_51:3, TAG_53:3, TAG_53:2, TAG_50:4, TAG_53:4, TAG_52:3, TAG_56:6, TAG_54:4, TAG_58:3, TAG_52:4, TAG_54:5, TAG_52:5, TAG_54:7, TAG_54:6, TAG_50:5, TAG_52:6, TAG_55:4, TAG_54:2, TAG_58:9, CE_18:2, CE_18:1, CE_16:0 and CE_22:6, which were increased due to hepatocyte-specific HuR deletion at steady-state, were also altered in the same manner in livers of HuR^{WT} mice upon feeding with the NAFLD-inducing diet (Figure-5E-G). In other words, the TAG lipidomic

phenotype of HuR-deficient livers at steady-state (genotype-driven change) is very similar to that of HuR^{WT} livers with NAFLD (diet-driven change, Figure-5G). In addition to phenocopying the TAG microenvironment of WT NAFLD livers (Figure-5G), the HuR-deficient livers at steady-state displayed a TAG signature similar to human NAFLD livers (27, 28). During human NAFLD, TAG_50:1 is enriched (28-31); similarly we found that this TAG was increased in HuR-deficient livers at steady-state (Figure-5E). Furthermore, TAG_48:0, TAG_52:3, TAG_54:4, TAG_52:4, TAG_54:5, TAG_56:6, TAG_52:5, TAG_54:7, TAG_54:2, CE_22:6 and CE_18:2, which were enhanced in HuR-deficient livers at steady-state (Figure-5E), are upregulated either in the liver or in circulation in human NAFLD (27, 28, 30, 31). Therefore, hepatocyte-specific HuR deficiency leads to a spontaneous phenotype that phenocopies the TAG signature within the hepatic microenvironment characteristic of human NAFLD. Lipidomic analysis of NAFLD livers (60%-HFD-CD feeding) revealed no differences in storage lipids between the two genotypes (Figure-5H-I). Together, hepatocyte HuR deficiency promotes the accumulation of storage lipids in the liver under steady-state conditions resulting in a lipidomic signature similar to that of wild-type livers with NAFLD as well as of human NAFLD livers.

The HuR-dependent hepato-protective network

Our phenotypic and multi-omic analysis demonstrated that hepatocyte-specific HuR deficiency promotes liver steatosis associated with a pro-fibrotic predisposition at steady-state, thereby leading to exacerbated fibrosis and HCC-like tumor development upon feeding a NAFLD-inducing diet. To mechanistically connect HuR functions as an RBP to RNA changes incurred by its deficiency in the liver, we next mapped the RNA interactors of HuR ribonucleoprotein (RNP) complexes in mouse livers by RNP-immunoprecipitation and RNA sequencing (RIP-seq). RIP was performed in cytoplasm-enriched extracts from healthy livers of wildtype mice using an anti-HuR antibody or an isotype matched IgG as control (Figure-S6A). Sequencing analysis of immunoprecipitated RNAs normalized to their expression values revealed 1380 mRNAs as enriched in HuR-RNPs with a fold change >1.5 and a $p<0.05$ over the IgG controls (Supplemental table-3). The quality of the RIP-seq was evaluated via the successful validation of 7 out of 8 mRNAs tested as HuR-RNP interactors in confirmatory qRT-PCRs from similarly immunoprecipitated

samples (Figure-S6B). Putative HuR targets were used to create functional pathway networks (Figure-6 and Supplemental tables-4-6).

Cytoplasmic HuR binds to its target mRNAs and promotes their use by augmenting mRNA stability or translation although in some cases it may act in a negative fashion (11, 32). Several target mRNAs from the RIP-seq were associated with hepatic metabolism, including glycerolipid, cholesterol, long chain fatty acid, monocarboxylic acid and carbohydrate metabolism (Figure-6 and Supplemental tables-4-6). The top most significant "Biological Process" identified via Gene Ontology analysis of the RIP-seq data was the monocarboxylic acid metabolic process, which contained 102 targets (Figure-6 and Supplemental table-5). In Gene Ontology, monocarboxylic acid metabolic process is a parent term for the bile acid metabolic process, among others. Thus, the RIP-seq findings are in agreement with the RNA-seq data, which showed that expression of genes involved in cholesterol biosynthesis and in the BA-activated FXR/RXR pathway were diminished due to hepatocyte HuR deficiency (Figure-2F-G).

The hepatic targets of HuR identified here are involved in various facets of BA metabolism and recycling. Besides mRNAs of genes mediating BA synthesis, such as *Cyp7a1* and *Cyp7b1*, HuR binds to mRNAs of transmembrane transporters of BA, such as *Abcc2*, *Slco1b2, Abcb11 and Slco1a4,* and of BA conjugating enzymes, such as *Slc27a2* (Supplemental table-3). We therefore measured BA levels in livers of HuR^{HepKO} and HuR^{WT} mice at steady-state. From the BAs that could be detected, taurochenodeoxycholic acid (TCDCA) and tauroursodeoxycholic acid (TUDCA) were downregulated in HuR-deficient livers compared to HuR sufficient livers (Figure-S7A-B). Noteworthy, both TUDCA and TCDCA have been shown to activate FXR (33, 34). Contrastingly, other BAs, such as tauromuricholic acid (alpha+beta) (TMCA α+β) or taurocholic acid (TCA) were not altered due to HuR deficiency (Figure-S7C-D).

Additionally, mRNAs regulating the function of the endoplasmic reticulum (ER), protein processing in the ER and ER stress response pathway were HuR targets (Figure-6 and Supplemental tables-3-6). IRE1α (encoded by *Ern1*), which is one of the arms of the unfolded protein response (UPR) and *Creb3l2*, which is a transcriptional activator

operative in the UPR, were HuR targets (Supplemental tables-3-6). Moreover, *Herpud1*, *Serp1*, *Amfr*, *Bfar*, *Herpud2*, *Atf4*, *Stub1*, *Vapb*, *Eif2ak2*, *Ep300* and *Hspa13*, which are genes that function in the ER's UPR are HuR targets (Supplemental tables-3-6). Hence, several of the factors and pathways identified here to be regulated by HuR in the liver, including the ER stress response, BA metabolism and FXR pathways, have been implicated in hepatic homeostatic metabolism and function, thereby portraying a central role of HuR in liver homeostasis (16-18, 35).

Continuing our search for protective pathways, which could fail in the absence of HuR, we sought to identify mRNAs that were bound to and regulated by HuR. Therefore, we compared the RNA-seq (Figure-2) with the RIP-seq data (Figure-6). Out of the 1049 genes that were significantly deregulated in HuR deficiency (Figure-2A), mRNAs of 110 genes were identified as HuR targets by RIP-seq (Figure-S8A), suggesting that HuR may bind to and regulate their use. Analysis of these 110 targets using the online automated meta-analysis tool, Metascape, revealed that the steroid biosynthetic process, cofactor metabolic process, biological oxidations, lipid homeostasis and protein folding were the top five enriched pathways (Figure S8B). The steroid biosynthetic process, which was the top significant pathway, further consisted of cholesterol metabolic process, sterol metabolic process, lipid biosynthetic process, metabolism of lipids, fatty acid metabolic process and monocarboxylic acid metabolic process as sub-categories, among others. The lipid homeostasis pathway consisted of plasma lipoprotein remodeling, lipid storage, lipid localization, cholesterol homeostasis, cholesterol efflux, triglyceride metabolic process, lipid transport and regulation of lipid localization as sub-categories, among others. However, pathways that are known to directly contribute to hepatic-fibrosis development were not enriched (Figure-S8B), thereby suggesting that the overrepresented hepatic fibrosis/HSC activation pathway due to hepatocyte-specific HuR deficiency (Figure-2B-C) is likely secondary to other alterations (e.g. in lipid metabolism) in hepatocytes. Hence, HuR regulates a hepato-protective lipid metabolic network in the liver, thereby maintaining lipid homeostasis and inhibiting NAFLD development and progression.

Osteopontin partially mediates fibrosis development in hepatocyte-specific HuR deficiency

Our data so far suggest that alterations in HuR-deficient hepatocytes may trigger HSC activation and fibrosis, possibly in a paracrine fashion. We therefore examined the RNA-seq data of HuR^{WT} and HuR^{HepKO} livers (Figure-2), in order to identify upregulation in HuR-deficient hepatocytes of mRNA of secreted factors that could contribute to HSC activation and fibrosis. Amongst other genes implicated in fibrosis development that were upregulated by hepatocyte-specific HuR deficiency, we chose to analyze the potential role of *Spp1* and its product osteopontin (OPN), as *Spp1* was within the top five significantly upregulated genes (ranked based on the adjusted p value) in HuR^{HepKO} livers, compared to HuR^{WT} livers (not shown), and as OPN is known to promote HSC activation and fibrogenesis (36, 37). Consistent with the RNA-seq data, qRT-PCR analysis verified that *Spp1* mRNA was increased in HuR^{HepKO} as compared to HuR^{WT} livers, both at steady state and upon 60%-HFD-CD diet feeding (Figure-7A-B). Additionally, primary hepatocytes from HuR^{HepKO} mice displayed higher OPN protein secretion than cells from HuR^{WT} mice (Figure-7C).

Previously, hepatocyte Notch activation was shown to induce fibrosis by increasing Sox9-dependent hepatocyte expression of OPN, which promotes HSC activation (36). Consistent with this study, *Hes1* and *Sox9*, which are downstream targets of the Notch pathway, and *Jag1*, which encodes the Notch ligand jagged-1, were significantly upregulated in HuR^{HepKO} livers compared to HuR^{WT} livers, based on the RNA-seq (not shown). The upregulation of *Hes1*, *Sox9* and *Jag1* expression in HuR^{HepKO} livers was confirmed by qRT-PCR (Figure-S9A-C). According to the RIP-seq analysis, *Jag1* is a direct target of HuR in the liver (Supplemental Table-3), suggesting that HuR may negatively regulate *Jag1* expression. Contrastingly, expression of other Notch pathway components, such as the Notch receptors 1-4, was unchanged in HuR-deficient livers (Figure-S9D-G). These findings indicate that due to the potential direct regulation of *Jag1* expression by HuR, hepatocyte-specific HuR deficiency results in upregulation of *Jag1* and of the Jag1/Notch-signaling pathway and consequently of *Spp1* expression and OPN secretion.

Therefore, we next addressed whether the increase in OPN may promote HSC activation and fibrosis owing to HuR deficiency. To this end, HuR^{HepKO} mice were treated with an OPN-neutralizing antibody, or control antibody, while being fed with 60%-HFD-CD diet. OPN blockade resulted in a tendency towards reduced fibrosis in HuR^{HepKO} mice, compared to control antibody treatment, as shown by picrosirius staining (Figure-7D-E). Additionally, qRT-PCR analysis for expression of fibrosis-related genes (Figure-S10) supported the partial reduction in fibrosis in HuR^{HepKO} mice by treatment with the OPN antibody. Together, increased OPN may, at least partially, mediate fibrosis development in hepatocyte-specific HuR deficiency.

DISCUSSION

We identified here hepatocyte HuR as an integral factor to the maintenance of liver metabolic homeostasis. We show that HuR regulates a network of homeostatic hepatic processes, including lipid and BA metabolism, thereby protecting against hepatic steatosis, fibrosis and HCC development. Strikingly, hepatocyte-specific HuR deficiency resulted in spontaneous hepatic steatosis, accumulation of a TAG signature resembling that of human NAFLD livers, HSC activation and predisposition to fibrosis. Hepatocyte-specific HuR-deficient mice on NAFLD-inducing diets displayed aggravated hepatic fibrosis and HCC-like tumor development. Hence, hepatocyte-specific HuR deficiency recapitulates the whole sequence of NAFLD pathology upto HCC development. Our findings unequivocally position HuR as a central player of hepatic homeostasis.

Cytoplasmic HuR interacts with its target mRNAs and either promotes mRNA stability, upregulates mRNA translation or can suppress either of those functions in specific tissues (10, 11, 32, 38). Here, we show that in cytoplasm-enriched liver fractions, HuR interacts with mRNAs of genes involved, amongst others, in lipid transport/metabolism, BA transport/metabolism, cholesterol metabolism, or the ER stress response pathway, hence, potentially regulating several homeostatic hepatic pathways. A comprehensive analysis involving transcriptomics, lipidomics and mass spectrometric BA measurement verified that HuR is a regulator of aforementioned metabolic pathways.

Lipidomic analysis revealed that the TAG species that were significantly increased at steady-state due to hepatocyte HuR deficiency were also increased in livers of WT mice upon feeding a NAFLD-inducing diet. Importantly, substantial similarities were observed between the storage lipid signature of HuR-deficient livers at steady-state and the lipidomic alterations in human NAFLD (27-31). TAG_48:0, TAG_50:1, TAG_52:3, TAG_54:4, TAG_52:4, TAG_54:5, TAG_56:6, TAG_52:5, TAG_54:7, TAG_54:2, CE_22:6 and CE_18:2, which were upregulated in HuR-deficient livers at steady-state, are upregulated in human NAFLD as well (27-31). Together, our findings demonstrate that the lipidomic signature of mouse NAFLD induced by the 60%-HFD-CD has substantial overlap with that from human NAFLD and is strikingly phenocopied by

deletion of a single RBP at steady-state. This finding suggests that HuR^{HepKO} mice may represent an appropriate model for studying NAFLD in the future.

The RIP-seq analysis showed that mRNAs of genes involved in BA synthesis, conjugation and transport are targets of HuR-RNPs. Specifically, the rate-limiting enzyme in BA synthesis *Cyp7a1*, the enzyme responsible for BA conjugation *Slc27a2*, and BA transporters *Abcb11*, *Slco1a4* and *Slco1b2,* among others, were HuR targets. We corroborated the RIP-seq data by measuring hepatic BA levels. The BA TCDCA and TUDCA were diminished in HuR-deficient livers at steady-state compared to HuR^{WT} livers. Previous studies have described the hepato-protective role of TUDCA in the context of NAFLD by inhibiting ER stress (39, 40), and treatment of genetically obese mice with TUDCA reduced hepatic steatosis by regulating genes involved in *de novo* lipogenesis (41). Both TUDCA and TCDCA are activators of FXR (33, 34); consistently, the BA-activated FXR/RXR pathway was overrepresented in the significantly downregulated genes in HuR-deficient livers, as assessed by RNA-seq. Hepatic FXR is a master regulator of lipid homeostasis and protects against NASH and its expression is inversely correlated to NASH severity (1). Together with previous findings that activation of FXR in hepatocytes leads to HuR upregulation (42), our present data may point to a possible feed-forward hepato-protective loop involving the FXR pathway and HuR.

Genes involved in the hepatic fibrosis/HSC activation pathway were upregulated in HuR-deficient livers at steady-state, reflecting the fibrosis predisposition due to HuR deficiency. However, mRNAs contributing to the hepatic fibrosis/HSC activation pathway that were upregulated in HuR-deficient livers were not cytoplasmic-targets of HuR in the liver. This suggests that the upregulated hepatic fibrosis/HSC activation pathway due to hepatocyte-specific HuR deficiency is likely secondary to the metabolic alterations in hepatocytes, as lipid accumulation in hepatocytes can promote HSC activation in a paracrine manner (4, 43-45). In support of the hypothesis that hepatocyte HuR regulates HSC activation and fibrosis in a paracrine fashion were our findings that HuR-deficient hepatocytes displayed higher *Spp1* expression and increased secretion of OPN, which promotes HSC activation and fibrosis (36) and that pharmacological OPN blockade in HuR^{HepKO} mice partially reduced liver fibrosis, compared to control antibody treatment. A

recent study demonstrated that pro-fibrotic OPN expression by hepatocytes is enhanced by hepatocyte Notch activation in a Sox9-dependent manner (36). Consistently, we found that the expression of the downstream targets of the Notch pathway, *Hes1* and *Sox9* were upregulated in HuR-deficient livers. Furthermore, expression of *Jag1,* encoding jagged-1, was elevated in HuR-deficient livers. Interestingly, we identified *Jag1* as a direct target of HuR in the liver by RIP-seq, suggesting that HuR may negatively regulate *Jag1* expression. Therefore, we conclude that activation of the Jag1/Notch-signaling pathway resulting in increased *Spp1* expression and OPN secretion due to hepatocyte HuR deficiency may, at least partially, mediate the increased HSC activation and fibrosis of HuR^{HepKO} mice compared to their HuR-sufficient littermates, although the contribution of further pro-fibrotic pathways cannot be excluded and merits further investigation. Furthermore, whether the disrupted lipid metabolism and/or the reduced FXR/RXR activation in HuR-deficient hepatocytes are functionally linked to the increased pro-fibrotic Jag1/Notch/OPN pathway requires future investigation.

Interestingly, long-term feeding with a NAFLD-inducing diet not only aggravated inflammation and fibrosis in HuR^{HepKO} mice, but, importantly, led to NASH-related HCC development in a portion of HuR^{HepKO} mice. Previous studies have shown that HuR was upregulated in livers from cirrhotic patients with HCC and that HuR inhibits apoptosis, promotes cell proliferation, cell cycle progression and hypoxia-induced glycolytic switch in HCC cells (23, 46-48). However, those studies have only investigated the function of HuR in HCC cells or in the context of established HCC. Our data show that hepatocyte-specific HuR deletion results in predisposition to NAFLD-related HCC. Hence, at steady-state, HuR exerts a protective function, supporting hepatocyte homeostasis.

The two NAFLD-inducing diets used in the present study (60%-HFD-CD and CD-HFD-45%) are based on choline deficiency and have therefore some limitations with regards to recapitulating human NAFLD pathology. It would be worth investigating the role of hepatocyte-specific HuR deficiency in the context of NAFLD development and progression by using alternative NAFLD/NASH-inducing diets, such as a high cholesterol diet complemented with fructose-containing drinking water (36, 44) in future studies. Notwithstanding these limitations, our present work defines HuR as a master regulator of

liver homeostasis, contributing to deceleration of diet-induced NASH and HCC development by regulating a hepato-protective metabolic network. Therefore, appropriate modulation of HuR actions could be harnessed therapeutically in the context of prevention of NAFLD-related sequelae.

ACKNOWLEDGMENTS

The authors thank Katharina Bär, Marta Prucnal, Sylvia Grossklaus and Stephan Friebe (Technische Universität Dresden) for technical assistance. The authors thank Vaggelis Harokopos (BSRC “Alexander Fleming”) for Next Generation Sequencing and Martin Reczko for initial bioinformatics analyses, Sofia Grammenoudi and Kleopatra Dagla for help with flow cytometry and biochemical analysis, Meropi Gennadi for help with histology and the InfrafrontierGR Infrastructure for providing animal housing, transgenic and genomic services at Fleming.

AUTHOR CONTRIBUTIONS

P.S. designed the study, performed experiments, analyzed and interpreted data and wrote the manuscript; S.G. performed experiments, analyzed and interpreted data and edited the manuscript; M.C., M.P, performed experiments and analyzed data; M.G., B.G., M.N., V.R.T., A.W, R.B., N.Z., P.M., K-J.C., M.A., I.P., V.N. performed experiments; Ales.P., M.L., Andr.P., A.S., I.K., A.D., R.H., A.M.J.D., I.H., A.D.P., analyzed data; J.H., U.C., interpreted data; D.L.K., co-designed the project, interpreted data, supervised research and edited the paper; T.C. designed the project, interpreted data, supervised research and wrote the manuscript.

DISCLOSURES

Ian Henry is now an employee of AstraZeneca.

António Miguel de Jesus Domingues is now an employee of Dewpoint Therapeutics.

REFERENCES

1. **Musso G, Cassader M**, Gambino R. Non-alcoholic steatohepatitis: emerging molecular targets and therapeutic strategies. Nat Rev Drug Discov 2016;15:249-274.
2. Rui L. Energy metabolism in the liver. Compr Physiol 2014;4:177-197.
3. Michelotti GA, Machado MV, Diehl AM. NAFLD, NASH and liver cancer. Nat Rev Gastroenterol Hepatol 2013;10:656-665.
4. Schwabe RF, Tabas I, Pajvani UB. Mechanisms of Fibrosis Development in Nonalcoholic Steatohepatitis. Gastroenterology 2020;158:1913-1928.
5. Donnelly KL, Smith CI, Schwarzenberg SJ, Jessurun J, Boldt MD, Parks EJ. Sources of fatty acids stored in liver and secreted via lipoproteins in patients with nonalcoholic fatty liver disease. J Clin Invest 2005;115:1343-1351.
6. Postic C, Girard J. Contribution of de novo fatty acid synthesis to hepatic steatosis and insulin resistance: lessons from genetically engineered mice. J Clin Invest 2008;118:829-838.
7. Benegiamo G, Mure LS, Erikson G, Le HD, Moriggi E, Brown SA, Panda S. The RNA-Binding Protein NONO Coordinates Hepatic Adaptation to Feeding. Cell Metab 2018;27:404-418 e407.
8. Laggai S, Kessler SM, Boettcher S, Lebrun V, Gemperlein K, Lederer E, Leclercq IA, et al. The IGF2 mRNA binding protein p62/IGF2BP2-2 induces fatty acid elongation as a critical feature of steatosis. J Lipid Res 2014;55:1087-1097.
9. Doller A, Pfeilschifter J, Eberhardt W. Signalling pathways regulating nucleo-cytoplasmic shuttling of the mRNA-binding protein HuR. Cell Signal 2008;20:2165-2173.
10. Grammatikakis I, Abdelmohsen K, Gorospe M. Posttranslational control of HuR function. Wiley Interdiscip Rev RNA 2017;8.
11. Lourou N, Gavriilidis M, Kontoyiannis DL. Lessons from studying the AU-rich elements in chronic inflammation and autoimmunity. J Autoimmun 2019;104:102334.
12. **Woodhoo A, Iruarrizaga-Lejarreta M**, Beraza N, Garcia-Rodriguez JL, Embade N, Fernandez-Ramos D, Martinez-Lopez N, et al. Human antigen R contributes to hepatic stellate cell activation and liver fibrosis. Hepatology 2012;56:1870-1882.
13. **Ge J, Chang N,** Zhao Z, Tian L, Duan X, Yang L, Li L. Essential Roles of RNA-binding Protein HuR in Activation of Hepatic Stellate Cells Induced by Transforming Growth Factor-beta1. Sci Rep 2016;6:22141.
14. **Zhang Z, Zong C,** Jiang M, Hu H, Cheng X, Ni J, Yi X, et al. Hepatic HuR modulates lipid homeostasis in response to high-fat diet. Nat Commun 2020;11:3067.
15. Stefan N, Haring HU. The metabolically benign and malignant fatty liver. Diabetes 2011;60:2011-2017.

16. **Sinal CJ, Tohkin M**, Miyata M, Ward JM, Lambert G, Gonzalez FJ. Targeted disruption of the nuclear receptor FXR/BAR impairs bile acid and lipid homeostasis. Cell 2000;102:731-744.

17. Watanabe M, Houten SM, Wang L, Moschetta A, Mangelsdorf DJ, Heyman RA, Moore DD, et al. Bile acids lower triglyceride levels via a pathway involving FXR, SHP, and SREBP-1c. J Clin Invest 2004;113:1408-1418.

18. Thomas C, Pellicciari R, Pruzanski M, Auwerx J, Schoonjans K. Targeting bile-acid signalling for metabolic diseases. Nat Rev Drug Discov 2008;7:678-693.

19. Cipriani S, Mencarelli A, Palladino G, Fiorucci S. FXR activation reverses insulin resistance and lipid abnormalities and protects against liver steatosis in Zucker (fa/fa) obese rats. J Lipid Res 2010;51:771-784.

20. Fiorucci S, Antonelli E, Rizzo G, Renga B, Mencarelli A, Riccardi L, Orlandi S, et al. The nuclear receptor SHP mediates inhibition of hepatic stellate cells by FXR and protects against liver fibrosis. Gastroenterology 2004;127:1497-1512.

21. Calkin AC, Tontonoz P. Transcriptional integration of metabolism by the nuclear sterol-activated receptors LXR and FXR. Nat Rev Mol Cell Biol 2012;13:213-224.

22. Moeini A, Cornella H, Villanueva A. Emerging signaling pathways in hepatocellular carcinoma. Liver Cancer 2012;1:83-93.

23. Kotta-Loizou I, Giaginis C, Theocharis S. Clinical significance of HuR expression in human malignancy. Med Oncol 2014;31:161.

24. Wolf MJ, Adili A, Piotrowitz K, Abdullah Z, Boege Y, Stemmer K, Ringelhan M, et al. Metabolic activation of intrahepatic CD8+ T cells and NKT cells causes nonalcoholic steatohepatitis and liver cancer via cross-talk with hepatocytes. Cancer Cell 2014;26:549-564.

25. Hassan HM, Isovic M, Kolendowski B, Bauer-Maison N, Onabote O, Cecchini M, Haig A, et al. Loss of Thymine DNA Glycosylase Causes Dysregulation of Bile Acid Homeostasis and Hepatocellular Carcinoma. Cell Rep 2020;31:107475.

26. Bergman S, Graeme-Cook F, Pitman MB. The usefulness of the reticulin stain in the differential diagnosis of liver nodules on fine-needle aspiration biopsy cell block preparations. Mod Pathol 1997;10:1258-1264.

27. Gorden DL, Myers DS, Ivanova PT, Fahy E, Maurya MR, Gupta S, Min J, et al. Biomarkers of NAFLD progression: a lipidomics approach to an epidemic. J Lipid Res 2015;56:722-736.

28. Alamri H, Patterson NH, Yang E, Zoroquiain P, Lazaris A, Chaurand P, Metrakos P. Mapping the triglyceride distribution in NAFLD human liver by MALDI imaging mass spectrometry reveals molecular differences in micro and macro steatosis. Anal Bioanal Chem 2019;411:885-894.

29. Oresic M, Hyotylainen T, Kotronen A, Gopalacharyulu P, Nygren H, Arola J, Castillo S, et al. Prediction of non-alcoholic fatty-liver disease and liver fat content by serum molecular lipids. Diabetologia 2013;56:2266-2274.

30. Sanders FWB, Acharjee A, Walker C, Marney L, Roberts LD, Imamura F, Jenkins B, et al. Hepatic steatosis risk is partly driven by increased de novo lipogenesis following carbohydrate consumption. Genome Biol 2018;19:79.

31. Yang RX, Hu CX, Sun WL, Pan Q, Shen F, Yang Z, Su Q, et al. Serum Monounsaturated Triacylglycerol Predicts Steatohepatitis in Patients with Non-alcoholic Fatty Liver Disease and Chronic Hepatitis B. Sci Rep 2017;7:10517.

32. Hinman MN, Lou H. Diverse molecular functions of Hu proteins. Cell Mol Life Sci 2008;65:3168-3181.

33. **Marquardt A, Al-Dabet MM,** Ghosh S, Kohli S, Manoharan J, ElWakiel A, Gadi I, et al. Farnesoid X Receptor Agonism Protects against Diabetic Tubulopathy: Potential Add-On Therapy for Diabetic Nephropathy. J Am Soc Nephrol 2017;28:3182-3189.

34. Wang H, Chen J, Hollister K, Sowers LC, Forman BM. Endogenous bile acids are ligands for the nuclear receptor FXR/BAR. Mol Cell 1999;3:543-553.

35. **Rutkowski DT, Wu J,** Back SH, Callaghan MU, Ferris SP, Iqbal J, Clark R, et al. UPR pathways combine to prevent hepatic steatosis caused by ER stress-mediated suppression of transcriptional master regulators. Dev Cell 2008;15:829-840.

36. Zhu C, Kim K, Wang X, Bartolome A, Salomao M, Dongiovanni P, Meroni M, et al. Hepatocyte Notch activation induces liver fibrosis in nonalcoholic steatohepatitis. Sci Transl Med 2018;10.

37. Bruha R, Vitek L, Smid V. Osteopontin - A potential biomarker of advanced liver disease. Ann Hepatol 2020;19:344-352.

38. Srikantan S, Gorospe M. UneCLIPsing HuR nuclear function. Mol Cell 2011;43:319-321.

39. Cho EJ, Yoon JH, Kwak MS, Jang ES, Lee JH, Yu SJ, Kim YJ, et al. Tauroursodeoxycholic acid attenuates progression of steatohepatitis in mice fed a methionine-choline-deficient diet. Dig Dis Sci 2014;59:1461-1474.

40. Ozcan U, Yilmaz E, Ozcan L, Furuhashi M, Vaillancourt E, Smith RO, Gorgun CZ, et al. Chemical chaperones reduce ER stress and restore glucose homeostasis in a mouse model of type 2 diabetes. Science 2006;313:1137-1140.

41. **Yang JS, Kim JT**, Jeon J, Park HS, Kang GH, Park KS, Lee HK, et al. Changes in hepatic gene expression upon oral administration of taurine-conjugated ursodeoxycholic acid in ob/ob mice. PLoS One 2010;5:e13858.

42. Singh AB, Dong B, Kraemer FB, Xu Y, Zhang Y, Liu J. Farnesoid X Receptor Activation by Obeticholic Acid Elevates Liver Low-Density Lipoprotein Receptor Expression by mRNA Stabilization and Reduces Plasma Low-Density Lipoprotein Cholesterol in Mice. Arterioscler Thromb Vasc Biol 2018;38:2448-2459.

43. **Wobser H, Dorn C,** Weiss TS, Amann T, Bollheimer C, Buttner R, Scholmerich J, et al. Lipid accumulation in hepatocytes induces fibrogenic activation of hepatic stellate cells. Cell Res 2009;19:996-1005.

44. Wang X, Cai B, Yang X, Sonubi OO, Zheng Z, Ramakrishnan R, Shi H, et al. Cholesterol Stabilizes TAZ in Hepatocytes to Promote Experimental Non-alcoholic Steatohepatitis. Cell Metab 2020;31:969-986 e967.

45. Wang X, Zheng Z, Caviglia JM, Corey KE, Herfel TM, Cai B, Masia R, et al. Hepatocyte TAZ/WWTR1 Promotes Inflammation and Fibrosis in Nonalcoholic Steatohepatitis. Cell Metab 2016;24:848-862.

46. **Cao C, Sun J,** Zhang D, Guo X, Xie L, Li X, Wu D, et al. The long intergenic noncoding RNA UFC1, a target of MicroRNA 34a, interacts with the mRNA stabilizing protein HuR to increase levels of beta-catenin in HCC cells. Gastroenterology 2015;148:415-426 e418.

47. Zhang LF, Lou JT, Lu MH, Gao C, Zhao S, Li B, Liang S, et al. Suppression of miR-199a maturation by HuR is crucial for hypoxia-induced glycolytic switch in hepatocellular carcinoma. EMBO J 2015;34:2671-2685.

48. Zhu H, Berkova Z, Mathur R, Sehgal L, Khashab T, Tao RH, Ao X, et al. HuR Suppresses Fas Expression and Correlates with Patient Outcome in Liver Cancer. Mol Cancer Res 2015;13:809-818.

Author names in bold designate co-first authorship.

FIGURE LEGENDS

Figure 1. Hepatocyte-specific HuR deletion promotes hepatic steatosis and fibrosis development

(A) H&E staining of livers from HuR^{WT} and HuR^{HepKO} mice at steady-state (fed a normal diet (ND) for 6 weeks). Scale bars, 100 μm.

(B) Representative images of H&E stained livers of HuR^{WT} and HuR^{HepKO} mice, which were fed a 60%-HFD-CD for 2 weeks. Scale bars, 100 μm.

(C) Representative images and (D) quantification of picrosirius red staining in livers of HuR^{WT} and HuR^{HepKO} mice, which were fed a 60%-HFD-CD for 2 weeks (2 w) or 6 weeks (6 w). Scale bars in C, 100 μm. HuR^{WT} mice fed a 60%-HFD-CD for 2 weeks, n = 7 mice; HuR^{HepKO} mice fed 60%-HFD-CD for 2 weeks, n = 10 mice; HuR^{WT} mice fed 60%-HFD-CD for 6 weeks, n = 11 mice; HuR^{HepKO} mice fed 60%-HFD-CD for 6 weeks, n = 12 mice. *P < 0.05, ***P < 0.001. Data are presented as mean ± s.e.m. Mann-Whitney U test.

(E) Quantification of hepatic hydroxyproline levels in HuR^{WT} and HuR^{HepKO} mice, which were fed a 60%-HFD-CD for 6 weeks. The data are presented as μg / mg of liver. HuR^{WT} mice, n = 11 mice; HuR^{HepKO} mice, n = 12 mice. **P < 0.01. Data are presented as mean ± s.e.m. Mann-Whitney U test.

(F left and F right) Genes encoding fibrosis-related molecules were analyzed by qRT-PCR in livers of HuR^{WT} and HuR^{HepKO} mice, which were fed a 60%-HFD-CD for 6 weeks. Gene expression was normalized to *B2m* (beta-2 microglobulin; F left) or *18S* (F right). Data are presented relative to the respective HuR^{WT} mice, set as 1. HuR^{WT} mice, n = 8 mice; HuR^{HepKO} mice, n = 5 mice. *Col1a1,* collagen type 1 alpha 1; *Sphk1*, sphingosine kinase 1; *Tgfb1*, transforming growth factor beta1; *Col3a1*, collagen, type III, alpha 1; *Col1a2*, collagen, type I, alpha 2; *Col4a5*, collagen, type IV, alpha 5; *Col4a2*, collagen, type IV, alpha 2; *Col4a1*, collagen, type IV, alpha 1; *Col6a3*, collagen, type VI, alpha 3; *Col4a4*, collagen, type IV, alpha 4; *Col27a1*, collagen, type XXVII, alpha 1; *Col6a1*, collagen, type VI, alpha 1; *Col5a2*, collagen, type V, alpha 2; *Pdgfd*, platelet-derived growth factor, D polypeptide; *Pdgfb*, platelet derived growth factor, B polypeptide; *Pdgfrb*, platelet derived growth factor receptor, beta polypeptide; *Timp2*, tissue inhibitor of metalloproteinase 2; *Tgfb2*, transforming growth factor, beta 2; *Igf1r*, insulin-like growth

factor I receptor. *P < 0.05, **P < 0.01. Data are presented as mean ± s.e.m. Mann-Whitney U test.

Figure 2. Fibrosis predisposition due to hepatocyte-specific HuR deletion

(A-G) RNA sequencing of livers from HuR^{WT} and HuR^{HepKO} mice at steady-state (fed a ND for 6 weeks) (n = 4 mice / group).

(A) Volcano plot shows the distribution of the adjusted P values (-Log10 (adjusted P value)) and the fold change (Log2 FC). Significantly upregulated genes are in red and downregulated genes are in blue, in total 593 genes were upregulated and 456 genes were downregulated in HuR^{HepKO} livers as compared to HuR^{WT} livers (adjusted P value < 0.05, Benjamini-Hochberg correction).

(B) Ingenuity pathway analysis (IPA) was performed using the significantly upregulated genes in the HuR^{HepKO} livers, as compared to HuR^{WT} livers (adjusted P value < 0.05, Benjamini-Hochberg correction). The top 25 enriched pathways are shown.

(C) Significantly upregulated genes in HuR^{HepKO} livers as compared to HuR^{WT} livers that belong to the hepatic fibrosis and hepatic stellate cell activation pathway were plotted in a heat map, using the online tool Morpheus. The colour scale represents the Z score.

(D) Gene set enrichment analysis (GSEA) shows a positive correlation between hepatocyte-specific HuR deficiency and extracellular matrix related genes. NES, normalized enrichment score.

(E) GSEA shows a positive correlation between hepatocyte-specific HuR deficiency and epithelial-mesenchymal transition related genes.

(F) IPA was performed using the significantly downregulated genes in the HuR^{HepKO} livers, as compared to HuR^{WT} livers (adjusted P value < 0.05, Benjamini-Hochberg correction). The top 25 overrepresented pathways in the significantly downregulated genes in the HuR^{HepKO} livers are shown.

(G) Significantly downregulated genes in HuR^{HepKO} livers as compared to the HuR^{WT} livers that belong to the FXR/RXR pathway were plotted in a heat map, using the online tool Morpheus. The colour scale represents the Z score.

(H) Confirmation qRT-PCR was performed with selected genes that were significantly upregulated or downregulated in the RNA sequencing (Panels A-G). Gene expression was normalized to *18S*. Data are presented relative to the respective expression in

HuR^{WT} mice, set as 1. *Pdgfb*, platelet derived growth factor B polypeptide; *Pdgfrb*, platelet derived growth factor receptor beta polypeptide; *Timp2*, tissue inhibitor of metalloproteinase 2; *Col1a1*, collagen type I alpha 1; *Col3a1*, collagen type III alpha 1; *Slc10a2*, solute carrier family 10 member 2; *Hpx*, hemopexin. n = 4 mice / group. *P < 0.05. Data are presented as mean ± s.e.m. Mann-Whitney U test.

Figure 3. Hepatocyte-specific HuR deletion promotes HCC-like tumor development in mice following long term CD-HFD-45% feeding

(A) Plasma AST and (B) ALT levels in HuR^{WT} and HuR^{HepKO} mice that were fed a CD-HFD-45% for 14 months. (C) Higher NASH activity score was calculated in HuR^{HepKO} livers as compared to HuR^{WT} livers after CD-HFD-45% feeding for 14 months. (D) Representative images of Masson Trichrome staining (MAS) performed in livers of HuR^{WT} and HuR^{HepKO} mice that were fed a CD-HFD-45% for 14 months. Scale bars, 100 µm. (E) Graph shows the presence (1) or absence (0) of tumors in livers of HuR^{WT} and HuR^{HepKO} mice that were fed a CD-HFD-45% for 14 months. In the HuR^{WT} group 0 / 27 mice developed tumors and in the HuR^{HepKO} group 9 / 54 mice developed tumors. (F) Representative histology image of a HCC-like tumor in a HuR^{HepKO} liver stained with H&E. Scale bar, 100 µm. (G) Representative image of a HCC-like tumor in a HuR^{HepKO} liver stained for AFP (alpha-fetoprotein). Scale bar, 100 µm. (H) Representative images of a HCC-like tumor in a HuR^{HepKO} liver stained for reticulin; the reticulin framework is typically reduced or incomplete in HCC. Different magnifications of the same tissue section are shown. Scale bars, 100 µm.

Data are presented as mean ± s.e.m. n = 27 mice in HuR^{WT} group and n = 54 mice in HuR^{HepKO} group. Mann-Whitney U test (A-C) or two-tailed Fisher's exact test (E). ****P < 0.0001,*P < 0.05.

Figure 4. Enhanced accumulation of immune cells in livers of HuR^{HepKO} mice following long term CD-HFD-45% feeding

(A) Inflammation score based on Batts-Ludwig system was performed in livers of HuR^{WT} and HuR^{HepKO} mice following CD-HFD-45% feeding for 14 months. N = 27 mice in HuR^{WT} group and n = 54 mice in HuR^{HepKO} group. (B-G) Flow cytometry analysis of $CD4^+$ T cells ($CD4^+CD8^-$), $CD8^+$ T cells ($CD8^+CD4^-$), $NK1.1^+$ NKT cells ($CD4^-CD8^-NK1.1^+$), neutrophils

($Gr1^+CD11b^+$), monocytes ($Gr1^-CD11b^+CD11c^-MHCII^-Ly6c^+$) and infiltrating macrophages ($Gr1^-CD11b^+CD11c^-MHCII^+Ly6c^+$) was performed in livers of HuR^{WT} and HuR^{HepKO} mice following CD-HFD-45% feeding for 14 months. n = 6 mice in HuR^{WT} group and n = 6 mice in HuR^{HepKO} group. ****P < 0.0001,*P < 0.05. Data are presented as mean ± s.e.m. Mann-Whitney U test.

Figure 5. A NAFLD-like hepatic lipid signature owing to hepatocyte HuR deficiency

(A-I) Lipidomic analysis of livers from HuR^{WT} and HuR^{HepKO} mice at steady-state (fed a ND for 6 weeks; n = 5 mice / group) and of livers from HuR^{WT} and HuR^{HepKO} mice with NAFLD (fed a 60%-HFD-CD for 2 weeks; n = 6 mice / group).

(A-E) Comparison of HuR^{WT} and HuR^{HepKO} mice at steady-state.

(A) Percentages of hepatic-storage lipids (TAG and CE) and non-storage lipids (all other lipid classes present in panel B except for TAG and CE) in HuR^{WT} and HuR^{HepKO} mice at steady-state, depicted as pie charts.

(B) Alterations in hepatic-lipid classes in HuR^{WT} and HuR^{HepKO} mice at steady-state, presented as mean pmol / µg of total protein. CE, cholesterol ester; Cer, ceramide; Chol, cholesterol; CL, cardiolipin; DAG, diacylglycerol; HexCer, hexosylceramide; LPA, lyso-phosphatidate; LPC, lyso-phosphatidylcholine; LPE, lyso-phosphatidylethanolamine; LPE O-, lyso-phosphatidylethanolamine-ether; LPI, lyso-phosphatidylinositol; LPS, lyso-phosphatidylserine; PA, phosphatidate; PC, phosphatidylcholine; PC O-, phosphatidylcholine-ether; PE, phosphatidylethanolamine; PE O-, phosphatidylethanolamine-ether; PG, phosphatidylglycerol; PI, phosphatidylinositol; PS, phosphatidylserine; SM, sphingomyelin; TAG, triacylglycerol. *P < 0.05. Data are presented as mean ± s.e.m.

(C) Principal component analysis (PCA) of hepatic-non-storage lipids (all other lipid classes present in panel B except for TAG and CE) from HuR^{WT} and HuR^{HepKO} mice at steady-state shows that the two conditions segregate along dimension 2, PC2. ***P < 0.001.

(D) PCA of hepatic-storage lipids (TAG and CE) from HuR^{WT} and HuR^{HepKO} mice at steady-state shows that the two conditions segregate along the first dimension, PC1. **P < 0.01.

(E) Alterations in storage lipid species (TAG and CE species) in the livers of HuR^{HepKO} mice at steady-state as compared to HuR^{WT} mice at steady-state. Y axis depicts the Log2 fold change of the lipids (HuR^{HepKO} / HuR^{WT}; Log2 FC was calculated using the pmol / µg values) and the X axis depicts the lipid species. Only the significantly ($P < 0.05$) altered storage lipid species are shown. The red color (in the font and in the outline of the bars) indicates the TAG and CE species that were also significantly altered in HuR^{WT} mice when fed a 60%-HFD-CD diet as compared to ND (data shown in panel F).

(F) Comparison of livers from HuR^{WT} mice with NAFLD (fed a 60%-HFD-CD) with HuR^{WT} mice at steady-state (fed a ND). The significantly ($P < 0.05$) altered storage lipid species (TAG and CE species) in the liver are shown. Y axis depicts the Log2 fold change of the lipids (60%-HFD-CD / ND; Log2 FC was calculated using the pmol / µg values) and the X axis depicts the lipid species. The red color (in the font and in the outline of the bars) indicates the TAG and CE species that were also significantly altered in the HuR-deficient livers as compared to HuR sufficient livers at steady-state (data shown in panel E).

(G) Storage lipid species, which were significantly upregulated in both comparisons (i) HuR^{WT} mice with NAFLD (fed a 60%-HFD-CD) as compared to HuR^{WT} mice at steady-state (fed a ND), hence, depicting 60%-HFD-CD-driven changes (as shown in panel F) and (ii) HuR^{HepKO} mice compared to HuR^{WT} mice at steady-state, hence, depicting genotype-driven changes (as shown in panel E), were plotted against each other using the Log2 fold change.

(H-I) Comparison of HuR^{WT} and HuR^{HepKO} mice with NAFLD (fed a 60%-HFD-CD).

(H) Hepatic-lipid classes in HuR^{WT} and HuR^{HepKO} mice with NAFLD (fed a 60%-HFD-CD), presented as mean pmol / µg of total protein. Abbreviations for the lipid classes are the same as in panel B. Data are presented as mean ± s.e.m.

(I) Percentages of hepatic-storage lipids (TAG and CE) and non-storage lipids (all lipid classes present in panel H except TAG and CE) in HuR^{WT} and HuR^{HepKO} mice with NAFLD (fed a 60%-HFD-CD).

Figure 6. Mapping the RNA interactors of HuR ribonucleoprotein complexes in the liver

RIP-seq was performed in healthy livers of WT C57BL/6 mice using a HuR antibody or an IgG control antibody. 1380 target mRNAs (fold change > 1.5, $P < 0.05$) interacted with

HuR and these HuR targets were used to create functional pathway networks (GO category biological process). The functional pathway networks presented here were generated from the GO category biological process. In addition to GO category biological process, the KEGG database and the GO category cellular component were used for mapping the HuR target mRNAs; the latter results are provided in supplemental tables 4-6. The package ClusterProfiler was used to perform GO term enrichment and network visualization. The enriched terms were defined as those that passed the following filters: P value < 0.01, q value < 0.05 and minGSSize > 10. Enrichment was tested using a hypergeometric test. To address the issue of false discovery rate, q values were calculated.

AA, amino acid; bio pro, biosynthetic process; cat pro, catabolic process; carb, carbohydrate; Chol, cholesterol; comp, compound; ER, endoplasmic reticulum; FA, fatty acid; LDL, low density lipoprotein; lip, lipid; met pro, metabolic process; pos reg, positive regulation; pro, process; pw, pathway; ROS, reactive oxygen species; reg, regulation; res, response; sig pw, signaling pathway; trans, transport; TCA, tricarboxylic acid; UP, unfolded protein; UPR, unfolded protein response; ubi, ubiquitination.

Figure 7. Osteopontin partially mediates fibrosis development in HuR^{HepKO} mice

(A) qRT-PCR analysis for *Spp1* (encoding for osteopontin, OPN) in livers of HuR^{WT} and HuR^{HepKO} mice, which were fed a ND for 6 weeks. *Spp1* gene expression was normalized to expression of *18s*. Data are presented relative to the HuR^{WT} mice, set as 1. n = 7 mice in HuR^{WT} group and n = 6 mice in HuR^{HepKO} group. **P < 0.01. Data are presented as mean ± s.e.m. Mann-Whitney U test.

(B) qRT-PCR analysis for *Spp1* in livers of HuR^{WT} and HuR^{HepKO} mice, which were fed a 60%-HFD-CD for 6 weeks. *Spp1* gene expression was normalized to expression of *18s*. Data are presented relative to the HuR^{WT} mice, set as 1. n = 8 mice in HuR^{WT} group and n = 5 mice in HuR^{HepKO} group. **P < 0.01. Data are presented as mean ± s.e.m. Mann-Whitney U test.

(C) Osteopontin (OPN) protein was measured in conditioned medium derived from HuR^{WT} or HuR^{HepKO} primary hepatocytes. N = 7. *P < 0.05. Data are presented as mean ± s.e.m. Mann-Whitney U test.

(D) Quantification and (E) representative images of picrosirius red staining in livers of HuR^{HepKO} mice, which were fed a 60%-HFD-CD for 2 weeks and treated with the osteopontin neutralizing antibody (OPN Ab) or control IgG antibody (IgG). n = 6 mice / group. Data are presented as mean ± s.e.m. Mann-Whitney U test. Scale bar, 100 μm.

Figure 1

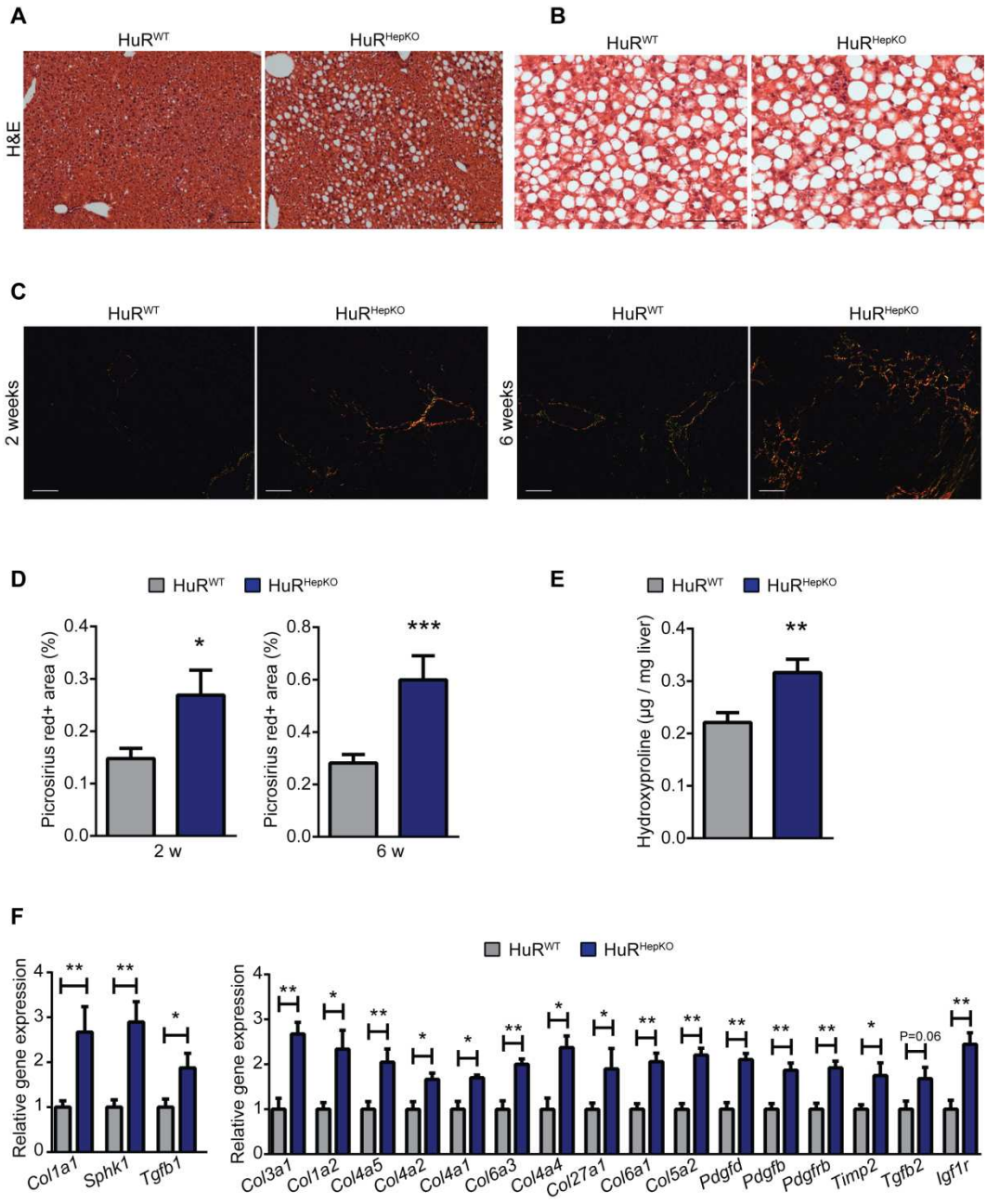

hep_32153_f1.tif

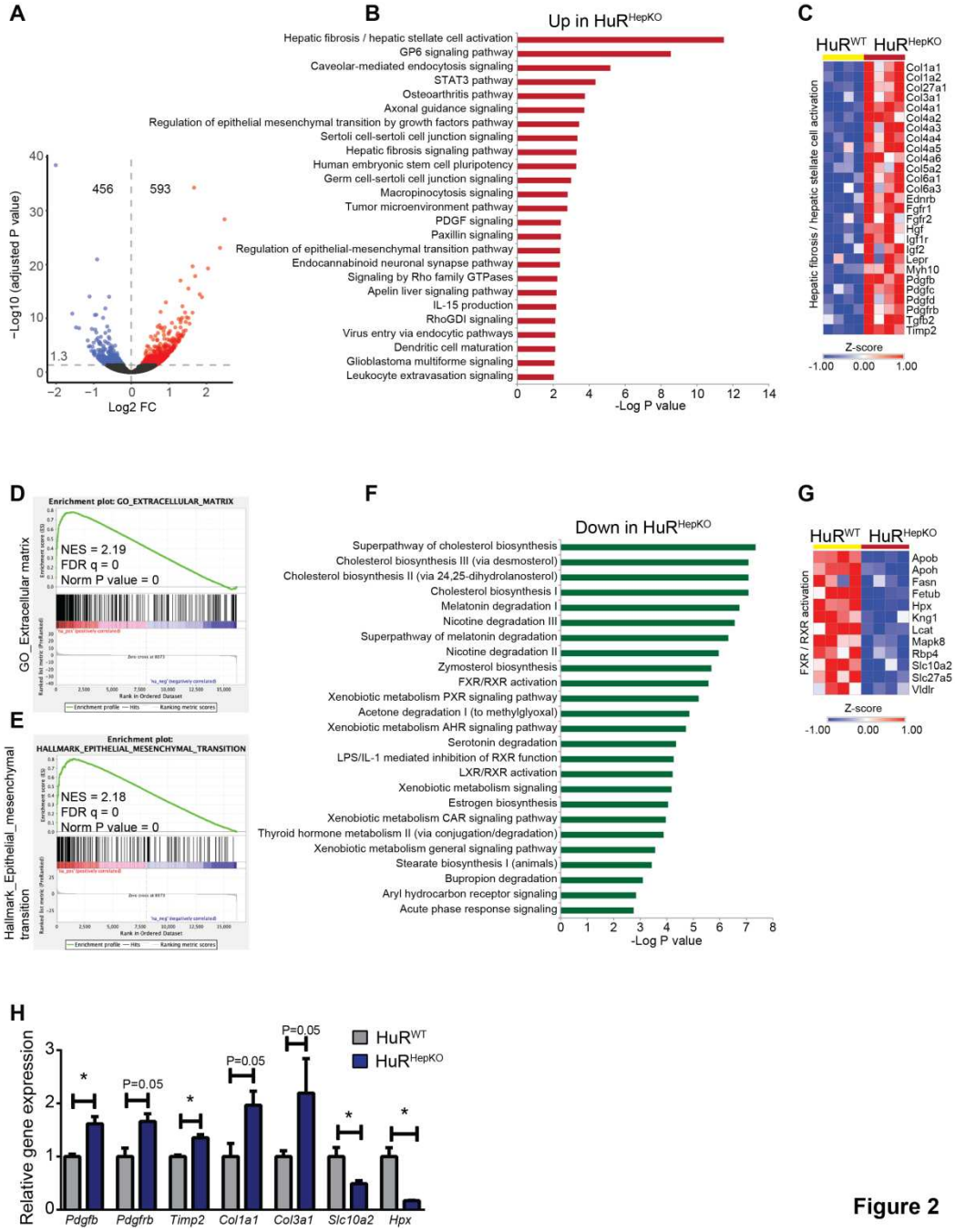

Figure 2

hep_32153_f2.tif

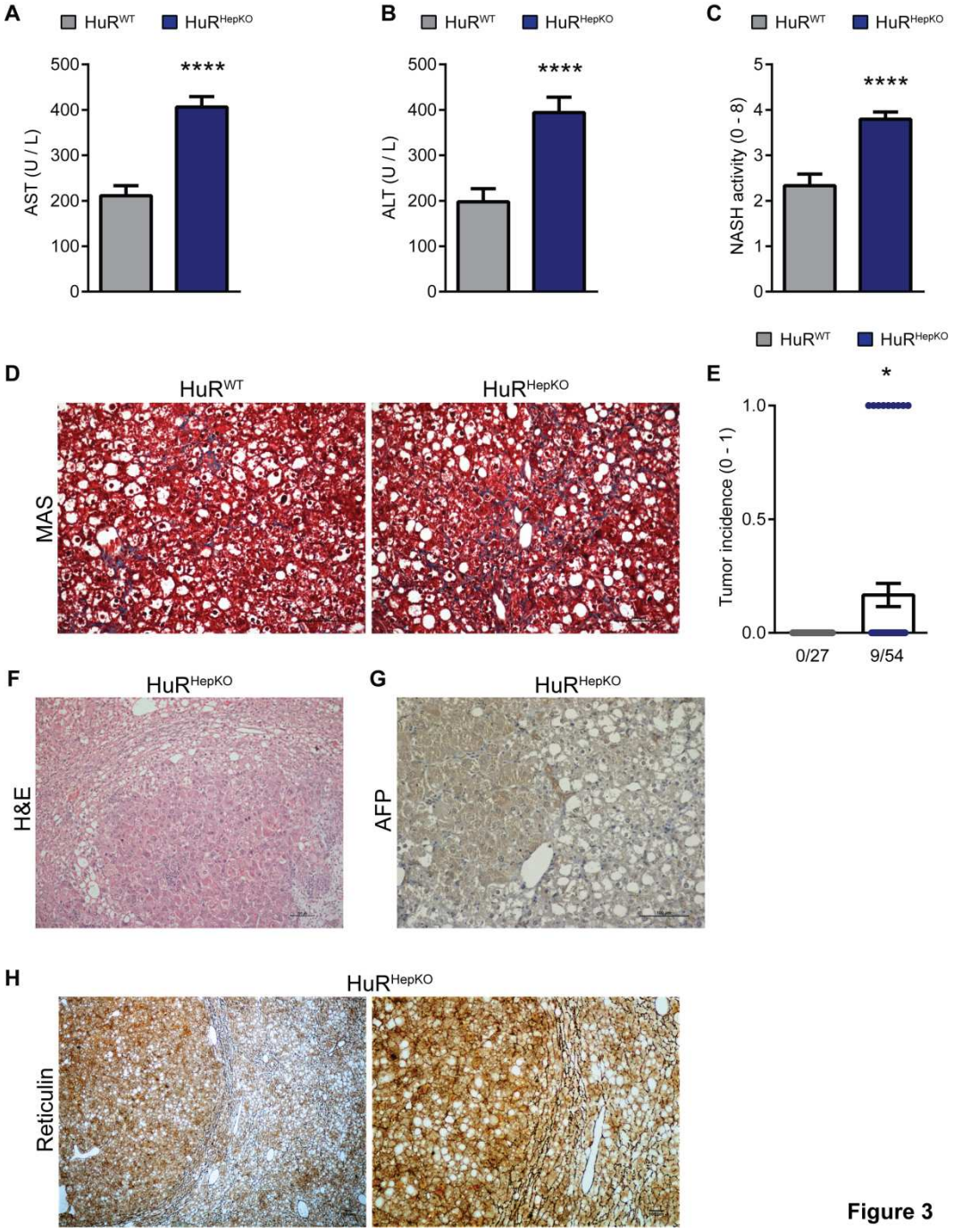

Figure 3

hep_32153_f3.tif

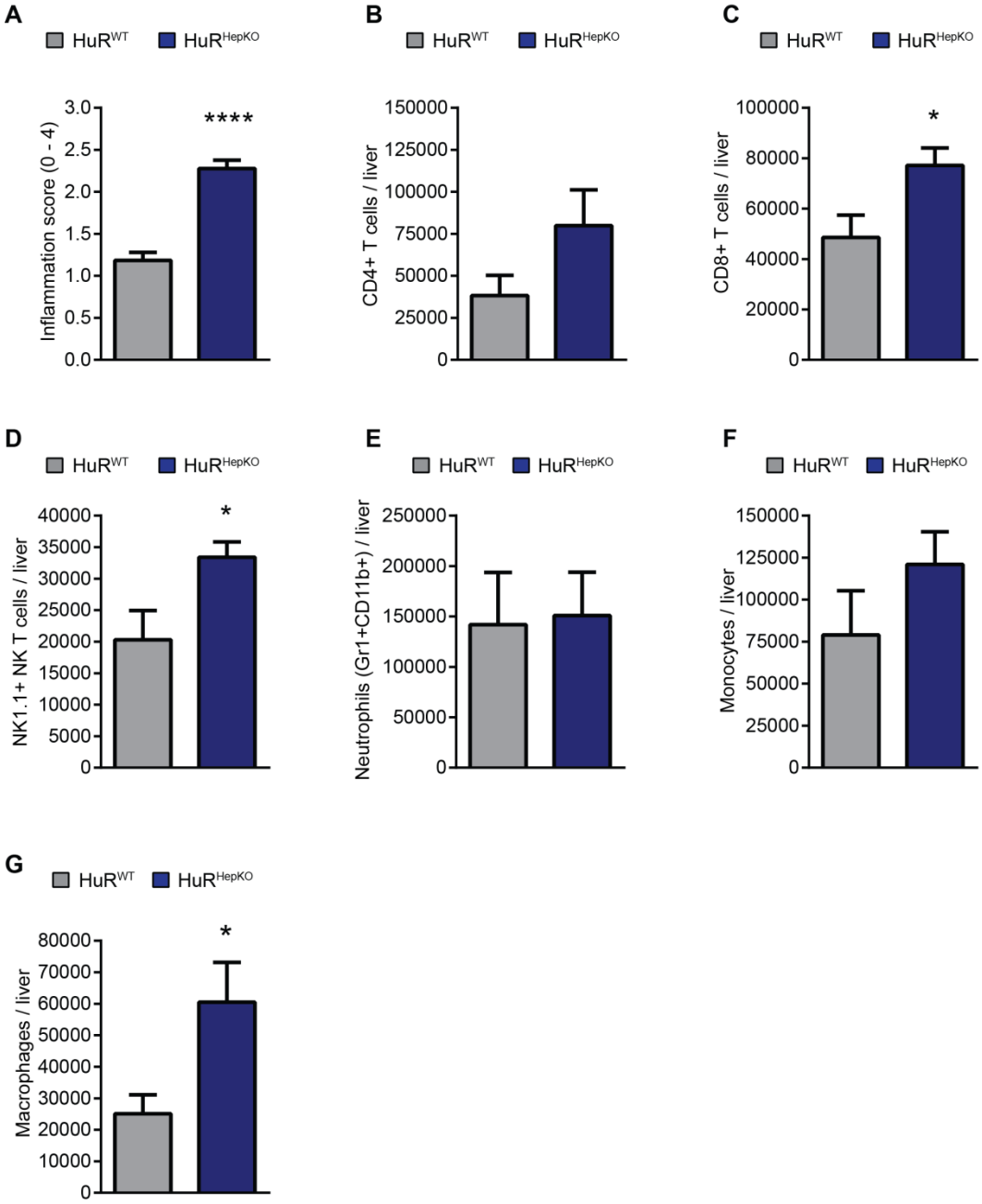

Figure 4

hep_32153_f4.tif

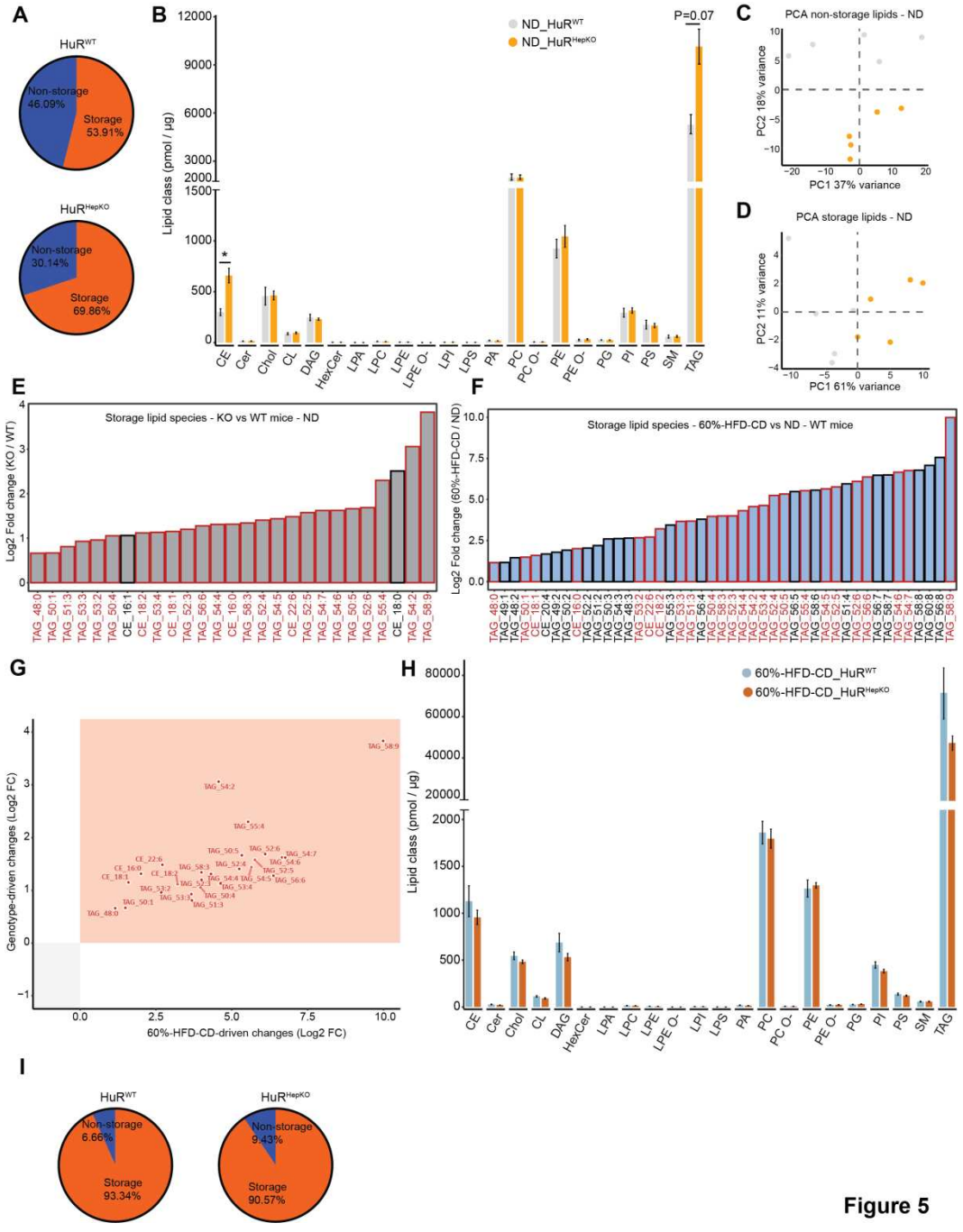

Figure 5

hep_32153_f5.tif

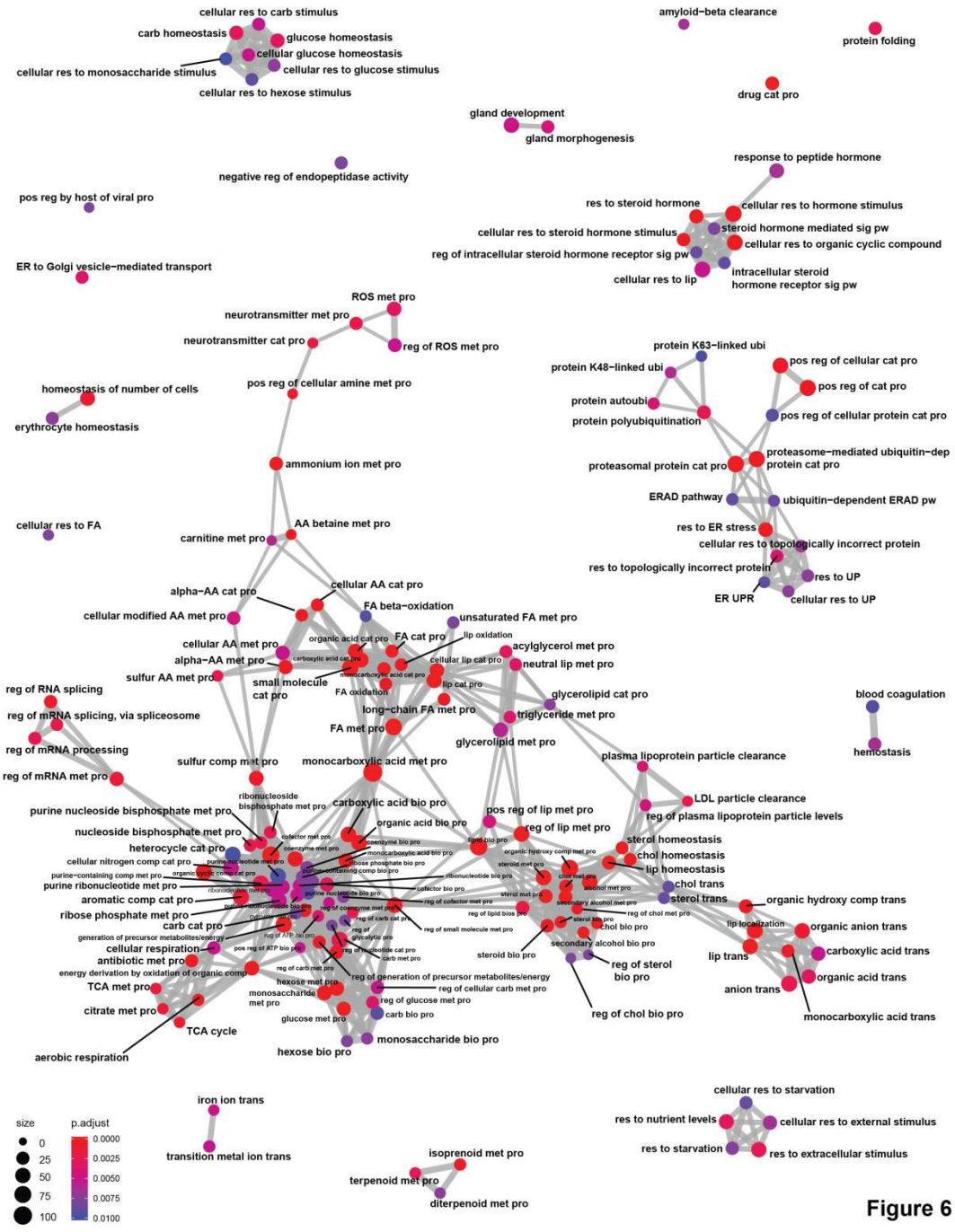

Figure 6

hep_32153_f6.tif

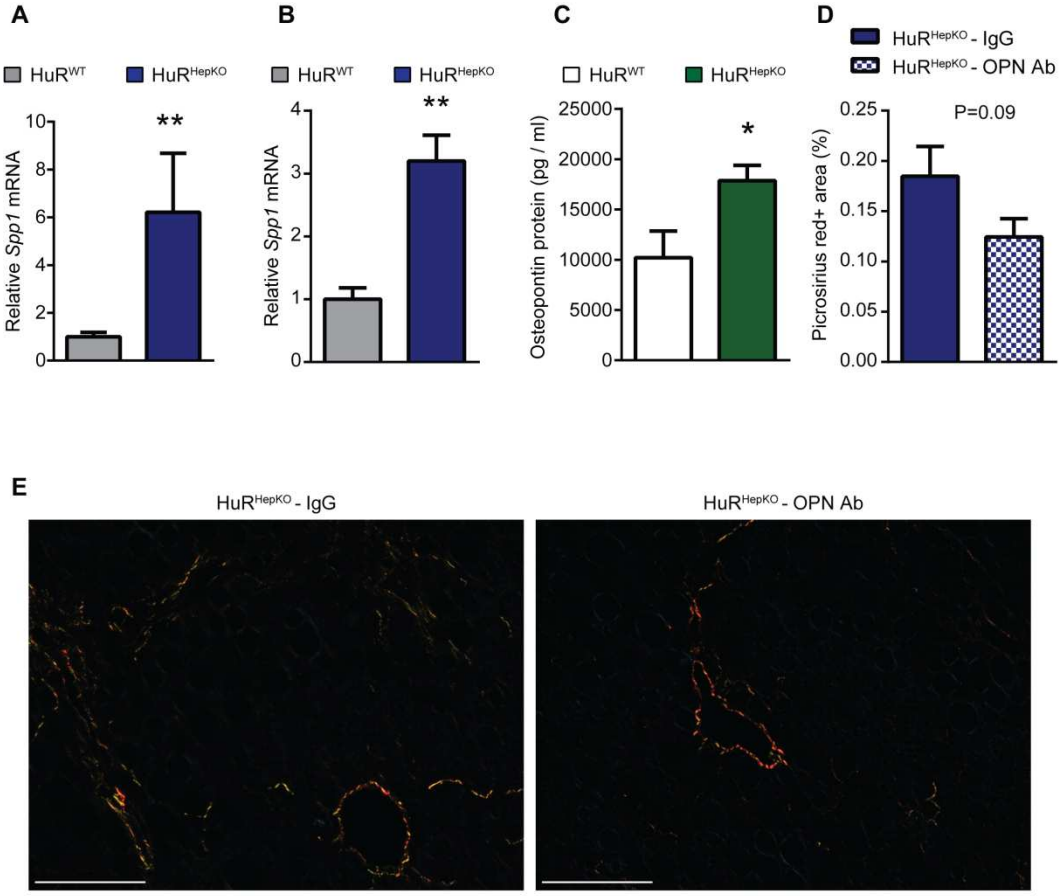

Figure 7

hep_32153_f7.tif